Received: 9 February 2022 | Revised: 24 May 2022 | Accepted: 20 July 2022

DOI: 10.33012/navi.558

ORIGINAL ARTICLE

Reconstructing GNSS Meta-Signal Observations Using Sideband Measurements

Daniele Borio* | **Ciro Gioia**

Joint Research Centre (JRC), European Commission, Ispra (VA), Italy

Correspondence
Daniele Borio
Enrico Fermi 2749
21027 Ispra (VA), Italy
Email: daniele.borio@ec.europa.eu

Summary

Global navigation satellite systems (GNSSs) provide several signals on different frequencies: Two or more components can be processed jointly as a meta-signal. Despite significant effort devoted to developing effective techniques for meta-signal processing, limited research has been conducted to characterize meta-signal measurements. In this work, the observations obtained by processing a GNSS meta-signal are characterized and fundamental relationships between GNSS meta-signal and dual-frequency measurement combinations are derived.

We show that subcarrier phase observations can be estimated as the wide-lane linear combination of the carrier phases obtained from the two original sideband components. Moreover, meta-signal code measurements can be reconstructed from the pseudoranges and carrier phases of the original components. Thus, meta-signal pseudoranges are mixed code and carrier observations. The experimental results confirm the validity of the theoretical formulas that can be used to reconstruct meta-signal measurements from dual-frequency observations.

Keywords

dual estimator, dual-frequency combinations, dual-phase estimator, GNSS meta-signal

1 | INTRODUCTION

Modern global navigation satellite systems (GNSSs) provide synchronous signals on multiple frequencies. This characteristic has opened several possibilities at both the measurement and signal processing levels. Significant work has been performed to optimally combine measurements from several frequencies (Deng et al., 2018; Li, 2018; Richert & El-Sheimy, 2007) in efforts to eliminate the impact of ionospheric delay, reduce noise, and improve the ambiguity resolution process in carrier-phase positioning. At the signal processing level, the concept of meta-signals (Issler et al., 2010; Paonni et al., 2014) has been introduced: A meta-signal is obtained when two (or more) GNSS components are considered together and processed as a single entity to obtain better tracking performance and high-accuracy code measurements. The two components forming the meta-signal must be on two different frequencies in order to obtain a composite signal with a Gabor bandwidth that is much wider than that of the original signals (Issler et al., 2010; Paonni et al., 2014). A large Gabor bandwidth is a precondition to

obtain high-accuracy code measurements (Betz & Kolodziejski, 2009) enabling high-accuracy code-based position solutions.

Meta-signal processing is inspired by binary offset carrier (BOC) and alternate binary offset carrier (Alt-BOC) modulations (Betz, 2001; Lestarquit et al., 2008) and, in particular, a generalized Alt-BOC modulation is created by combining signals from two different frequencies. The original sideband components can be interpreted as the two main spectral lobes of a BOC/Alt-BOC modulation and, similar to the BOC/Alt-BOC cases, the joint processing of signals from different carrier frequencies leads to ambiguous code measurements.

While the potential of meta-signal processing has been demonstrated, for example, through the analysis of the Cramer-Rao lower bound (CRLB; Das et al., 2020; Ortega et al., 2020), meta-signals have a multi-peaked correlation function and a tracking loop can lock on a secondary peak, leading to biased measurements (Nardin et al., 2020; Schwalm et al., 2020). The number of secondary correlation peaks increases with the frequency separation of the sideband components and false locks can significantly degrade meta-signal processing performance (Schwalm et al., 2020). Moreover, filtering and other non-idealities can worsen the ambiguity problem that should be addressed with dedicated algorithms (Nardin et al., 2020). In this respect, tracking a meta-signal is a problem similar to that of BOC/Alt-BOC processing. Additional correlators are needed either to detect and avoid false peak locks (Fine & Wilson, 1999) or to track the subcarrier in an independent manner (Borio, 2014; Hodgart & Blunt, 2007; Yao et al., 2017).

Significant research has been conducted to solve the meta-signal ambiguity problem. These efforts have found, for example, direct applications to the processing of BeiDou navigation satellite system (BDS)-3 signals. With the completion of the BDS-3 phase, B1I and B1C signals are broadcast in the L1 band with close center frequencies. These components will be multiplexed into one composite signal and can thus be considered a meta-signal. In this respect, research (Gao et al., 2020a, 2020b; Wang et al., 2017; Zhang et al., 2019) has been performed to develop tracking algorithms that optimally exploit the benefits of the wideband B1 signal and solve the ambiguity problem. Wang et al. (2017) extended the double estimator (DE)/double phase estimator (DPE) algorithm to avoid the ambiguity problem and demonstrated improved tracking performance for the B1 composite signal. Zhang et al. (2019) proposed the wideband high-accuracy joint tracking technique (WHAT), which further optimizes the algorithm introduced by Wang et al. (2017) and reduces the number correlators.

In Gao et al. (2020a, 2020b), cross-aided tracking (CAT) is introduced. Additionally in this case, a dedicated loop, the subcarrier phase lock loop (SPLL), is used to track the subcarrier component and to avoid correlation secondary peaks. In this manner, three loops are used to track the code, the carrier, and the subcarrier components. A delay lock loop (DLL) is used to track the code component and provides raw delay estimates that can be converted into low-accuracy pseudoranges. In the following, this type of measurement is denoted as raw pseudoranges. Final code measurements are then obtained by combining the outputs of the SPLL and DLL. The third loop, the phase lock loop (PLL), is used to track the carrier component in a manner similar to that in standard receiver architectures (Kaplan & Hegarty, 2017; Van Dierendonck, 1997).

These papers show that a meta-signal can be effectively processed using an additional subcarrier loop, which avoids the code ambiguity problem by separately tracking the subcarrier component. This receiver architecture, in which three loops are used, is denoted in the following as a generalized double phase estimator (GDPE) as it extends the DE/DPE approaches proposed by Hodgart and Blunt (2007) and Borio (2014), respectively.

In addition to the techniques already noted, additional solutions for solving the ambiguity problem have been investigated, for example, considering a vector receiver architecture (García-Molina, 2021; García-Molina & Fernández-Rubio, 2019) in which the code ambiguities of all signals in view are solved simultaneously in a vector solution. In Hameed et al. (2021), the ambiguity problem is solved using a modified least-squares ambiguity decorrelation (LAMBDA) method.

Despite these efforts, meta-signals have been analyzed primarily in the signal processing domain and a characterization in terms of final measurements has not been completed. The analysis provided in this paper fills this gap and derives fundamental relationships between GNSS meta-signal and dual-frequency measurement combinations (Hofmann-Wellenhof et al., 2001).

More specifically, by comparing the measurements generated by the separate processing of the sideband components and the observations obtained using the GDPE on the corresponding meta-signal, we derive fundamental relationships between the two sets of observations. In particular, the subcarrier phase of a meta-signal is shown to be equivalent to the wide-lane linear combination of the carrier phases obtained from the two sideband components. The raw meta-signal pseudorange is also shown to be a linear combination of the pseudoranges obtained from the original sideband components. The weights of this linear combination depend on both the power and slope of the main peak of the correlation functions of the individual sideband signals. The sideband component received with the highest power and with the steepest correlation function is weighted the most. When the two components are characterized by the same modulation and by the same received power, the average of the sideband pseudoranges is found. Finally, the meta-signal carrier phase is shown to be the narrow-lane carrier phase combination of the sideband carrier-phase observations.

After establishing the different relationships between meta-signals and sideband observations, we adopted the approach proposed by Hodgart and Blunt (2007) and used elsewhere (Gao et al., 2020a, 2020b; Wang et al., 2017; Zhang et al., 2019) to compute the final high-accuracy pseudoranges. In this respect, we show that high-accuracy pseudoranges equivalent to those obtained through meta-signal processing can be found by combining carrier phases and pseudoranges from sideband components. Thus, meta-signal pseudoranges cannot be considered pure code measurements. Instead, they are code observations smoothed using the wide-lane linear combination of the sideband carrier phases.

The relationships derived should not be intended as strict identities because meta-signal and sideband measurements are generated by different tracking loop architectures with different loop parameters. Thus, differences may arise due to the non-linear tracking behavior resulting, for instance, in possible carrier/subcarrier cycle slips. Different processing strategies result in different impacts of thermal noise, multipath, and dispersive propagation effects on meta-signal and reconstructed measurements. Here, equivalence has to be intended in a statistical sense. It is better discussed in Section 5 where it is shown that the reconstructed measurements have statistical properties (mean and standard deviation) similar to those of the corresponding meta-signal observations.

More specifically, theoretical results have been supported by experiments conducted using real measurements from the Alt-BOC signal and its sideband components. In particular, a Septentrio PolaRx5S receiver was configured to simultaneously process the full Galileo E5 Alt-BOC and its sideband components. In this manner, it was possible to simultaneously log measurements for the two processing options (combined and separate processing). Carrier smoothing was disabled to obtain pseudoranges only from the code component. Alt-BOC observations and measurements reconstructed from sideband components were compared, showing

a good agreement and supporting the validity of the theoretical results derived in the paper. Analysis in the position domain showed that the position solution obtained using final pseudoranges reconstructed from the sideband observations practically coincides with the position solution obtained from full Alt-BOC processing.

These results support the theoretical findings developed in the paper and show that measurements and position solutions obtained using meta-signal processing can be reconstructed using the observations obtained from the individual sideband components.

The methodology developed to reconstruct meta-signal observations can also be applied to other signal processing approaches introduced to improve the quality of code measurements. For instance, Pany and Yang (2017) discussed code and carrier tracking techniques for spectrally asymmetric signals including the variable IF tracking loop (VITAL) approach introduced by Yang (2016). In the VITAL architecture, a residual intermediate-frequency (IF) component is left on the signal provided as input to the DLL. This signal has an asymmetric spectrum and a Gabor bandwidth larger than that of the corresponding baseband signal. Moreover, this signal is characterized by a sharper correlation function with multiple peaks. Thus, the VITAL DLL has to be able to avoid false secondary peak locks. The approach developed here enables the reconstruction of the measurements provided by techniques such as VITAL and, in particular, it allows one to show that VITAL code measurements are observations smoothed using carrier-phase information. This type of analysis is left for future work.

This paper is an extended version of Borio and Gioia (2022) and provides additional analysis with the comparison between measurements from Alt-BOC processing and reconstructed from the sideband observations.

The remainder of this paper is organized as follows: Section 2 introduces the basic concepts behind GNSS meta-signals and their processing using a GDPE architecture. Equivalence formulas linking measurements from sideband and meta-signal processing are derived in Section 3. The experimental setup is described in Section 4. Experimental results are provided in Section 5. Finally, Section 6 concludes the paper.

2 | GNSS META-SIGNALS AND DPE

In meta-signal processing, two separate components on two different frequencies, $x(t)$ and $y(t)$, are considered jointly as a single signal with a wide Gabor bandwidth. This principle is illustrated in Figure 1, in which $x(t)$ denotes the signal with lower center frequency, f_1, representing the lower sideband component of the resulting meta-signal. $y(t)$ is the upper sideband component with center frequency f_2.

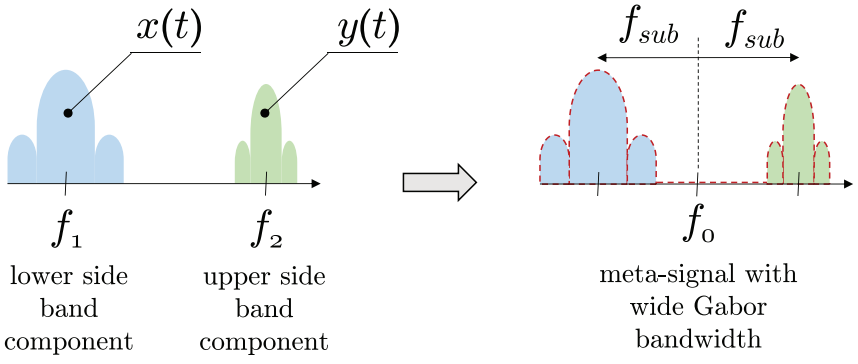

FIGURE 1 Two GNSS signals can be considered jointly as a single meta-signal characterized by a wide Gabor bandwidth.

The center frequency of the meta-signal is given by:

$$f_0 = \frac{f_1 + f_2}{2} \tag{1}$$

and is the average between f_1 and f_2. The frequency f_0 is equal to half the frequency of the narrow-lane combination:

$$f_0 = \frac{1}{2} f_N \tag{2}$$

The interaction between the two sideband components also forms a complex subcarrier characterized by the subcarrier frequency:

$$f_{sub} = \frac{f_2 - f_1}{2} \tag{3}$$

The subcarrier of BOC/Alt-BOC signals introduces secondary peaks in the signal autocorrelation function. Thus, the DLL, which is used to estimate the signal delay (pseudorange) by maximizing the signal autocorrelation function, can lock onto a secondary peak, leading to ambiguous code delay measurements. A possible solution was introduced (Hodgart & Blunt, 2007; Hodgart et al., 2008) with the DE in which two different delays are estimated for the subcarrier and code components, respectively. In this manner, an ambiguous correlation is mapped into an unambiguous function of two variables. The estimated code and subcarrier delays are then recombined in a single measurement.

The approach introduced by Hodgart and Blunt (2007) and Hodgart et al. (2008) was further developed by Borio (2014) with the introduction of the DPE. The basic principle of the DPE is to approximate a BOC signal as the composition of two side lobes that need to be aligned in phase before being summed and processed jointly. In the DPE, the subcarrier is assimilated to a carrier component, which is tracked with a modified PLL. As previously discussed, DE/DPE processing can be applied to meta-signals as demonstrated by Gao et al. (2020a, 2020b), Wang et al. (2017), and Zhang et al. (2019).

DPE can also be implemented as a form of coherent sideband processing (Borio, 2017; Feng et al., 2016). This last approach should be adopted for meta-signals because each sideband component is characterized by its own spreading code and, thus, correlation has to be performed separately on the two sideband signals (Nardin et al., 2020; Paonni et al., 2014).

In standard processing (Kaplan & Hegarty, 2017), each sideband component is processed independently using a PLL/DLL architecture in which each signal is correlated with a local code and carrier replica and a complex correlator is found for each component. While in the following, only the prompt correlator is considered, similar considerations apply also to the early and late correlators.

The prompt correlators obtained from this process can be expressed as (Kaplan & Hegarty, 2017):

$$\begin{aligned} P_1 &= A_1 R_1(\tau - \tau_1)\exp\{j2\pi(\varphi - \varphi_1)\} + \eta_1 \\ &= A_1 R_1(\Delta\tau_1)\exp\{j2\pi\Delta\varphi_1\} + \eta_1 \\ P_2 &= A_2 R_2(\tau - \tau_2)\exp\{j2\pi(\varphi - \varphi_2)\} + \eta_2 \\ &= A_2 R_2(\Delta\tau_2)\exp\{j2\pi\Delta\varphi_2\} + \eta_2 \end{aligned} \tag{4}$$

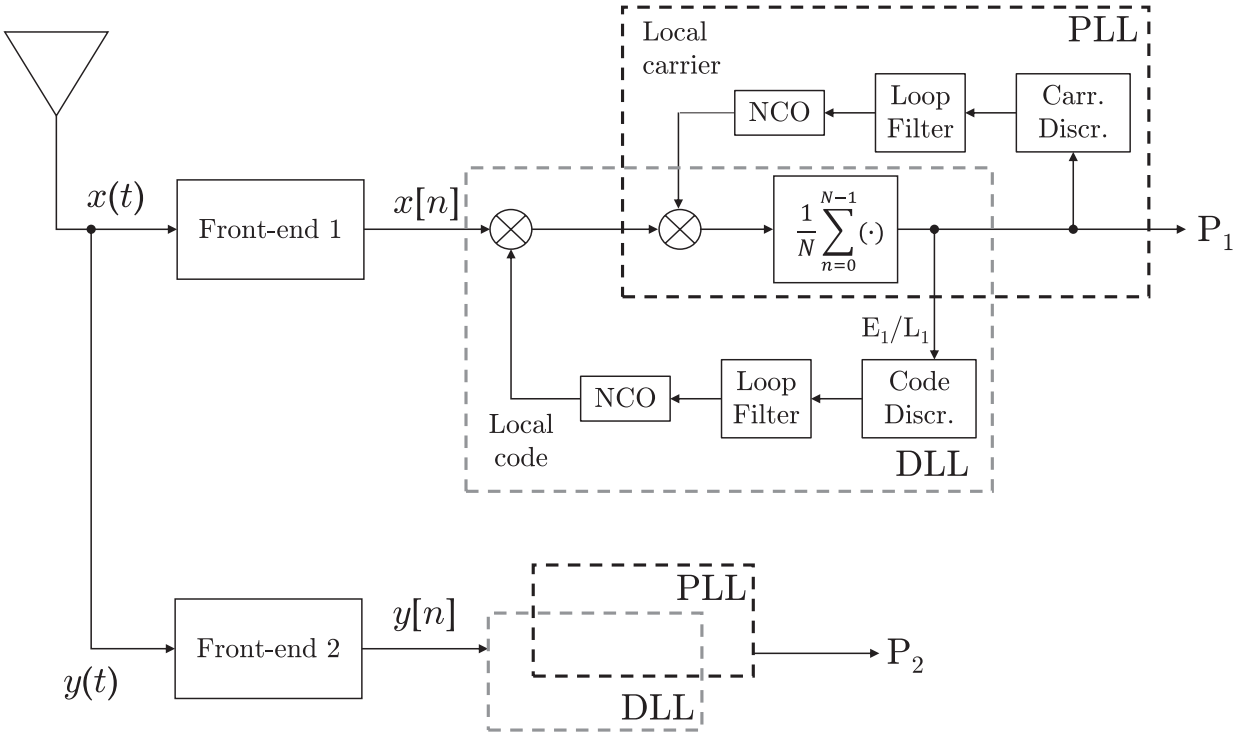

FIGURE 2 Schematic representation of standard GNSS tracking with a DLL/PLL architecture applied independently to the two sideband components

where A_1 and A_2 are the correlator amplitudes and $R_1(\cdot)$ and $R_2(\cdot)$ are the signal correlation functions. In Equation (4), τ_1 is the delay of the local code used to process the lower sideband component, τ is the actual signal delay, and $\Delta\tau_1 = \tau - \tau_1$ is the residual delay difference. Similarly, φ_1 is the phase used for the local carrier generation, φ is the actual carrier phase, and $\Delta\varphi_1 = \varphi - \varphi_1$ is the residual phase error. The same definitions apply to quantities with index two that are related to the upper sideband component. η_1 and η_2 are two independent noise terms. In Equation (4), the impact of residual Doppler frequency errors has been neglected. Moreover, data bits are not considered; they can be either estimated for data signals or not present, for example, in pilot-only processing.

The basic principles of independent sideband processing are depicted in Figure 2, which provides a schematic representation of the standard DLL/PLL receiver architecture. Some details, such as the computation of the early and late correlators, have been omitted for ease of representation. A detailed review of tracking loop principles is out of the scope of this paper and can found in any GNSS textbook such as Kaplan and Hegarty (2017). In Figure 2, the two sideband components are processed independently and independent estimates are found for the code delays, τ_1 and τ_2, and for the carrier phases, φ_1 and φ_2.

When the meta-signal processing is applied and the same delay in both sideband components is exploited to jointly process the two signals. This method alleviates constraints on the code delays and carrier phases. A precondition for the meta-signal processing is that the two front-ends used to bring the sideband components to baseband are synchronized and driven by the same local oscillator.

A possible architecture for meta-signal processing (Gao et al., 2020a, 2020b) is shown in Figure 3. In this case, the correlators obtained from the two sideband

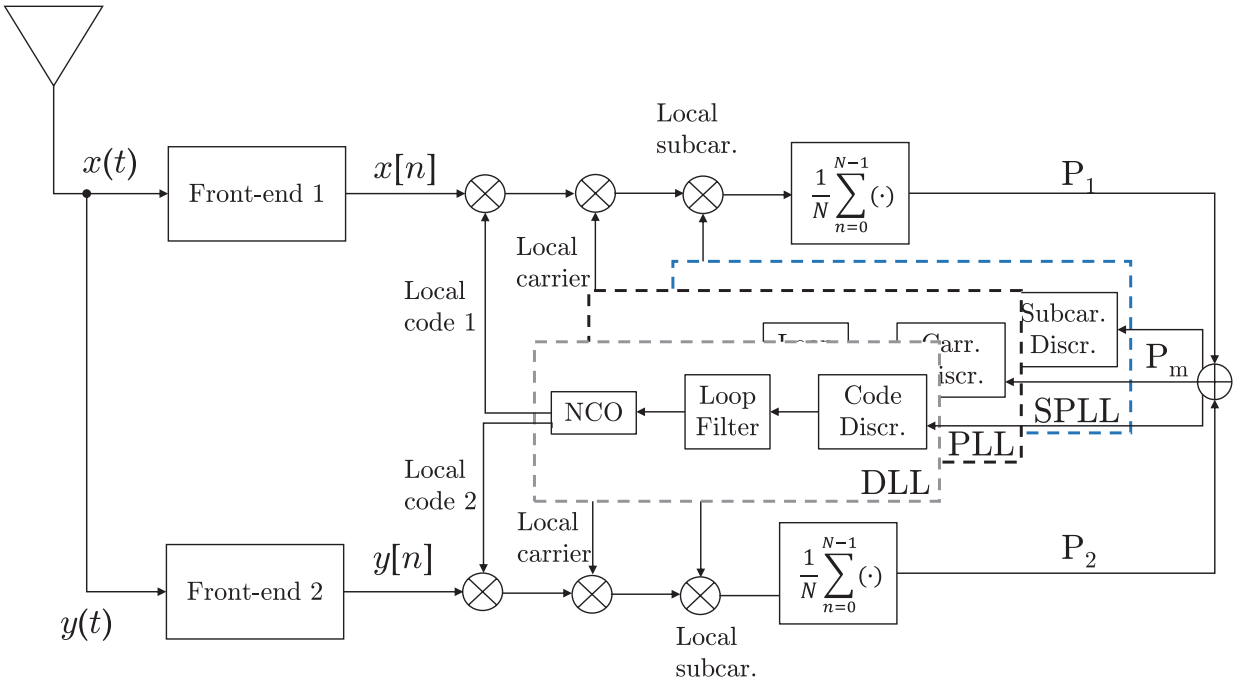

FIGURE 3 Schematic representation of coherent meta-signal processing using a triple-loop architecture

components are coherently summed to obtain a single meta-signal correlator output.

The meta-signal correlator output can be expressed using Equation (4) as:

$$\begin{aligned}
P_m &= P_1 + P_2 = A_1 R_1(\Delta\tau_1) e^{j2\pi\Delta\varphi_1} + \eta_1 + A_2 R_2(\Delta\tau_2) e^{j2\pi\Delta\varphi_2} + \eta_2 \\
&= \left[A_1 R_1(\Delta\tau_1) + A_2 R_2(\Delta\tau_2)\right] \frac{e^{j2\pi\Delta\varphi_1} + e^{j2\pi\Delta\varphi_2}}{2} \\
&+ \left[A_1 R_1(\Delta\tau_1) - A_2 R_2(\Delta\tau_2)\right] \frac{e^{j2\pi\Delta\varphi_1} - e^{j2\pi\Delta\varphi_2}}{2} + \eta \\
&= R_s e^{j2\pi\frac{\Delta\varphi_1+\Delta\varphi_2}{2}} \frac{e^{j2\pi\frac{\Delta\varphi_1-\Delta\varphi_2}{2}} + e^{-j2\pi\frac{\Delta\varphi_1-\Delta\varphi_2}{2}}}{2} \\
&+ R_d e^{j2\pi\frac{\Delta\varphi_1+\Delta\varphi_2}{2}} \frac{e^{j2\pi\frac{\Delta\varphi_1-\Delta\varphi_2}{2}} - e^{-j2\pi\frac{\Delta\varphi_1-\Delta\varphi_2}{2}}}{2} + \eta \\
&= R_s e^{j2\pi\Delta\varphi_0} \cos\left(2\pi\Delta\varphi_{sub}\right) + jR_d e^{j2\pi\Delta\varphi_0} \sin\left(2\pi\Delta\varphi_{sub}\right) + \eta
\end{aligned} \tag{5}$$

where

- R_s is the sum of the correlation terms:

$$R_s = A_1 R_1\left(\Delta\tau_1\right) + A_2 R_2\left(\Delta\tau_2\right) \tag{6}$$

- R_d is the difference of the correlation terms:

$$R_d = A_1 R_1\left(\Delta\tau_1\right) - A_2 R_2\left(\Delta\tau_2\right) \tag{7}$$

- $\eta = \eta_1 + \eta_2$ is the overall noise term:
- $\Delta\varphi_0$ is the residual meta-signal carrier phase error:

$$\Delta\varphi_0 = \frac{\Delta\varphi_1 + \Delta\varphi_2}{2} \tag{8}$$

- $\Delta\varphi_{sub}$ is the residual meta-signal subcarrier phase error:

$$\Delta\varphi_{sub} = \frac{\Delta\varphi_1 - \Delta\varphi_2}{2} \tag{9}$$

The term:

$$R_m = R_s \cos\left(2\pi\,\Delta\varphi_{sub}\right) + jR_d \sin\left(2\pi\,\Delta\varphi_{sub}\right) \tag{10}$$

defines a complex correlation function, which is considered in Paonni et al. (2014) as the correlation function of the meta-signal. In the previous derivation, two different estimated delays, τ_1 and τ_2, were still assumed. However, for the architecture in Figure 3, the same delay is adopted for the two sideband components and $\Delta\tau_1 = \Delta\tau_2 = \Delta\tau$. This delay error is tracked by the DLL, whereas the residual carrier and subcarrier errors, $\Delta\varphi_0$ and $\Delta\varphi_{sub}$, are respectively estimated by the PLL and SPLL depicted in Figure 3. Using a triple-loop architecture such as that shown in Figure 3 avoids ambiguities in the code correlation function (Gao et al., 2020a, 2020b). For instance, in Paonni et al. (2014), the residual subcarrier-phase error is also expressed as:

$$\Delta\varphi_{sub} = f_{sub}\,\Delta\tau \tag{11}$$

Thus, the residual subcarrier and delay errors are jointly estimated. Using Equation (11), the meta-signal correlation function provided in Paonni et al. (2014) is obtained:

$$\begin{aligned} R_m(\Delta\tau) = &\left[A_1 R_1(\Delta\tau) + A_2 R_2(\Delta\tau)\right]\cos\left(2\pi f_{sub}\,\Delta\tau\right) \\ &+ j\left[A_1 R_1(\Delta\tau) - A_2 R_2(\Delta\tau)\right]\sin\left(2\pi f_{sub}\,\Delta\tau\right) \end{aligned} \tag{12}$$

The cosine term in Equation (12), $\cos\left(2\pi f_{sub}\,\Delta\tau\right)$, introduces a narrow peak around $\Delta\tau = 0$, leading to a correlation function significantly sharper than the individual sideband correlation functions. However, the oscillations of this cosine term introduce secondary peaks in the correlation function leading to the ambiguity problem. This problem is solved using a triple-loop architecture such as that shown in Figure 3. The ambiguity problem can be solved by avoiding constraining the subcarrier residual phase error as in Equation (11). When the subcarrier component is properly recovered, the imaginary part of Equation (10) disappears and the correlation function of the meta-signal becomes a linear combination of the sideband correlation functions.

As for the sideband processing case, some details were omitted from Figure 3 for ease of representation. The detailed processing of meta-signals using the DPE framework is out of the scope of this paper and more details can be found in the references provided above. In the next section, Equation (5) will be used to establish the equivalence between meta-signal measurements and linear combinations of observations from the sideband components.

3 | EQUIVALENT MEASUREMENT MODEL

When a meta-signal is processed using a GDPE architecture, three residual errors, the meta-signal code delay, $\Delta\tau$, the residual subcarrier phase, $\Delta\varphi_{sub}$, and the residual meta-signal phase, $\Delta\varphi_0$, are estimated by the three loops depicted in Figure 3. These errors are in turn used to determine GNSS observables such as carrier phases and pseudoranges.

In particular, $\Delta\tau$ is used to estimate the signal transmit time that is built in a piecewise manner to exploit the time of week (ToW) that is extracted from the navigation message, as well as additional synchronization information depending on the structure of the specific GNSS signal considered (Kaplan & Hegarty 2017). For instance, the Global Positioning System (GPS) coarse acquisition (C/A) signal is organized in subframes lasting 6 seconds. Each subframe contains a handover word (HoW) with the ToW. Moreover, each subframe is made of 300 bits. At a given instant, expressed with respect to the receiver time, it is possible to estimate the transmission time from the ToW, the number of bits in the current subframe, the number of code periods in the current bit, and the residual code delay derived from $\Delta\tau$. A pseudorange is finally computed as the difference between the receiver time and the corresponding transmission time (Kaplan & Hegarty, 2017; Tsui, 2004). Thus, pseudoranges can be obtained from $\Delta\tau$ by adding/subtracting several additional terms. Details on the construction of pseudoranges from the residual delay errors can be found in previous studies (Kaplan & Hegarty, 2017; Tsui, 2004). In the following, pseudoranges are denoted as ρ_i with $i = 0, 1,$ and 2, where subscript 0 indicates quantities related to the meta-signal, and indexes 1 and 2 refer to observations from the sideband components. Pseudoranges are obtained from delay errors through the addition of proper correction terms; thus, relationships obtained for $\Delta\tau$ can be directly expressed in terms of ρ_i.

Carrier-phase observations, denoted as φ_1 and φ_2 for the sideband components, are obtained by integrating the corresponding tracking errors.

In the following, we provide equations describing the tracking errors obtained when considering sideband and meta-signal processing. These relationships are then expressed in terms of carrier-phase and pseudorange observables and can be used as reconstruction formulas to obtain meta-signal measurements from sideband observations.

3.1 | Carrier Phase

Equation (13) defines how the meta-signal carrier phase is formed. In particular, it directly follows from Equation (8):

$$\varphi_0 = \frac{\Phi_0}{\lambda_0} = \frac{1}{2}\left(\varphi_1 + \varphi_2\right) = \frac{1}{2}\left(\frac{\Phi_1}{\lambda_1} + \frac{\Phi_2}{\lambda_2}\right) \tag{13}$$

where φ_0 is the meta-signal carrier phase expressed in cycles. $\Phi_0, \Phi_1,$ and Φ_2 are carrier-phase measurements expressed in meters obtained by normalizing observations in cycles by the related wavelengths: λ_0 for the meta-signal, λ_1 for the lower sideband component, and λ_2 for the upper sideband component.

The relationship between measurements in meters is easily found as:

$$\Phi_0 = \frac{\lambda_0}{2}\left(\frac{\Phi_1}{\lambda_1} + \frac{\Phi_2}{\lambda_2}\right) = \frac{c}{2f_0}\left(\frac{f_1\Phi_1}{c} + \frac{f_2\Phi_2}{c}\right) = \frac{f_1\Phi_1 + f_2\Phi_2}{2f_0} = \frac{f_1\Phi_1 + f_2\Phi_2}{f_1 + f_2} \tag{14}$$

where c is the speed of light. Equation (14) shows that the meta-signal carrier phase is the narrow-lane carrier-phase combination (Hofmann-Wellenhof et al., 2001) of the sideband carrier-phase observations. Note that carrier-phase measurements are ambiguous in terms of integer multiples of cycles (Hofmann-Wellenhof et al., 2001). When the reconstruction formula from Equation (13) is applied, a division by two is performed. This implies that ambiguities of integer multiples of half-cycles affect the reconstructed carrier phase, φ_0. When this ambiguity is expressed in meters, it implies that Φ_0 can be reconstructed up to an integer multiple of $\frac{\lambda_0}{2}$, which is the effective wavelength of a narrow-lane carrier-phase combination.

3.2 | Subcarrier Phase

Similar to the previous case, the model for subcarrier measurements can be derived from Equation (9):

$$\begin{aligned}\varphi_{sub} &= \frac{\Phi_{sub}}{\lambda_{sub}} = \frac{1}{2}\left(\varphi_2 - \varphi_1\right) = \frac{1}{2}\left(\frac{\Phi_2}{\lambda_2} - \frac{\Phi_1}{\lambda_1}\right)\\ \Phi_{sub} &= \frac{\lambda_{sub}}{2}\left(\frac{\Phi_2}{\lambda_2} - \frac{\Phi_1}{\lambda_1}\right) = \frac{c}{2f_{sub}}\left(\frac{f_2\Phi_2}{c} - \frac{f_1\Phi_1}{c}\right)\\ &= \frac{f_2\Phi_2 - f_1\Phi_1}{2f_{sub}} = \frac{f_2\Phi_2 - f_1\Phi_1}{f_2 - f_1}\end{aligned} \tag{15}$$

where φ_{sub} is the subcarrier phase expressed in cycles. Φ_{sub} is the same measurement expressed in meters. These equations show that φ_{sub} is the wide-lane combination (Hofmann-Wellenhof et al., 2001) of the sideband carrier-phase observations.

Regarding the carrier phase case, reconstructed subcarrier phases will suffer an ambiguity of integer multiples of either half-cycles or $\frac{\lambda_{sub}}{2}$, depending on whether they are expressed in cycles or in meters. $\lambda_w = \frac{\lambda_{sub}}{2}$ is the wavelength of a wide-lane carrier-phase combination.

3.3 | Pseudorange Measurements

When the subcarrier phase is properly recovered, Equation (10) becomes:

$$R_m = R_s = A_1 R_1\left(\Delta\tau_1\right) + A_2 R_2\left(\Delta\tau_2\right) \tag{16}$$

In meta-signal processing, $\Delta\tau_1$ and $\Delta\tau_2$ are constrained to have the same value, $\Delta\tau$. The equivalence between sideband processing and meta-signal processing measurements can be obtained by stipulating that the measurements from the two cases lead to the same correlation values:

$$A_1 R_1(\Delta\tau) + A_2 R_2(\Delta\tau) = A_1 R_1\left(\Delta\tau_1\right) + A_2 R_2\left(\Delta\tau_2\right) \tag{17}$$

In order to solve Equation (17), $\Delta\tau, \Delta\tau_1$, and $\Delta\tau_2$ are assumed to be close to zero so that for such values R_1 and R_2 can be approximated as ideal triangles:

$$R_i(\tau) = 1 - \alpha_i|\tau|, \qquad i = 1, 2 \tag{18}$$

where α_i is the slope of the main peak of the i-th correlation function. In binary phase shift keying (BPSK) modulated signals, α_i is the inverse of the chip duration. A sharper correlation function leads to a larger α_1. In this manner, Equation (17) becomes:

$$A_1\left(1-\alpha_1\left|\Delta\tau\right|\right)+A_2\left(1-\alpha_2\left|\Delta\tau\right|\right)=A_1\left(1-\alpha_1\left|\Delta\tau_1\right|\right)+A_2\left(1-\alpha_2\left|\Delta\tau_2\right|\right) \tag{19}$$

which implies:

$$\left|\Delta\tau\right|=\frac{\alpha_1 A_1}{\alpha_1 A_1+\alpha_2 A_2}\left|\Delta\tau_1\right|+\frac{\alpha_2 A_2}{\alpha_1 A_1+\alpha_2 A_2}\left|\Delta\tau_2\right| \tag{20}$$

Equation (20) indicates that the residual code error in meta-signal processing can be expressed as the weighted mean of the code errors in the single sideband components. Components with sharper correlation functions or those that are received with a larger amplitude should be weighted more. Assuming that the residual code errors all have the same sign, Equation (20) becomes:

$$\Delta\tau=\frac{\alpha_1 A_1}{\alpha_1 A_1+\alpha_2 A_2}\Delta\tau_1+\frac{\alpha_2 A_2}{\alpha_1 A_1+\alpha_2 A_2}\Delta\tau_2 \tag{21}$$

This relationship can be directly expressed in terms of pseudoranges as:

$$\rho_0=\frac{\alpha_1 A_1}{\alpha_1 A_1+\alpha_2 A_2}\rho_1+\frac{\alpha_2 A_2}{\alpha_1 A_1+\alpha_2 A_2}\rho_2 \tag{22}$$

where ρ_0 is the pseudorange obtained for the meta-signal and ρ_1 and ρ_2 are the pseudoranges obtained for the sideband components.

For a symmetric modulation such as the Alt-BOC, it is possible to assume that the received signal amplitudes A_1 and A_2 are equal. Moreover, the two sideband components are characterized by the same modulation and $\alpha_1=\alpha_2$. In such case:

$$\rho_0=\frac{1}{2}\left(\rho_1+\rho_2\right) \tag{23}$$

3.4 | High-Accuracy Pseudoranges

In the previous sections, DPE processing was assumed and three components, including the subcarrier phase, were considered. However, as discussed by Hodgart and Blunt (2007) and Hodgart et al. (2008), the final code delay estimate should be obtained by combing code and subcarrier measurements. Equation (16) of Hodgart and Blunt (2007) defines a basic strategy to obtain the final code delay. This strategy can be adopted here and the final high-accuracy meta-signal pseudorange can be computed as:

$$\rho^{+}=\lambda_w\ \text{round}\left(\frac{\rho_0-\rho^{*}}{\lambda_w}\right)+\rho^{*} \tag{24}$$

where $\lambda_w=\frac{c}{2f_{sub}}=\frac{\lambda_{sub}}{2}$ is the wavelength of the wide-lane combination of the sideband components. The item $\text{round}\left(\cdot\right)$ is the round function and provides the closest integer to its argument.

ρ^* is obtained from the subcarrier phase, Φ_{sub}, as:

$$\rho^* = \Phi_{sub} - \lambda_w \,\text{round}\left(\frac{\Phi_{sub}}{\lambda_w}\right) \tag{25}$$

ρ^* is the fractional part of of the subcarrier phase and assumes values in $\left[-\lambda_w/2, \lambda_w/2\right]$, whereas $\text{round}\left(\frac{\rho_0-\rho^*}{\lambda_w}\right)$ can be interpreted as a simple estimator, based on ρ_0, of the wavelength ambiguity of Φ_{sub}.

Equation (24) has been obtained by expressing the DE recombining equation (Hodgart & Blunt, 2007) in terms of pseudoranges and carrier-phase measurements. Subcarrier measurements reconstructed using Equation (15) are ambiguous in terms of multiples of λ_w and this fact is thus accounted for in Equation (24).

Other approaches including subcarrier smoothing can be adopted to obtain high-accuracy pseudorange measurements.

Importantly, the final meta-signal pseudorange measurement is not only derived from code components but is obtained by combining pseudoranges with subcarrier phases. This is in line with the previously noted discussion stating that improved accuracy comes from the cosine term introduced by the subcarrier component.

4 | EXPERIMENTAL SETUP AND ANALYSIS

The theoretical results derived in the previous sections were supported by experiments conducted using real GNSS carrier-phase and pseudorange measurements. More than 4 hours of data were collected using a Septentrio PolaRx5S receiver connected to a rooftop antenna whose location was carefully surveyed. These data were used to support the validity of the theory developed. GNSS observations were collected under static open-sky conditions. Additional tests in suburban and urban scenarios will be considered in future work.

A schematic representation of the setup adopted for the data collection and analysis is provided in Figure 4. The Septentrio PolaRx5S receiver is able to collect measurements from the E5a and E5b bands and simultaneously process the

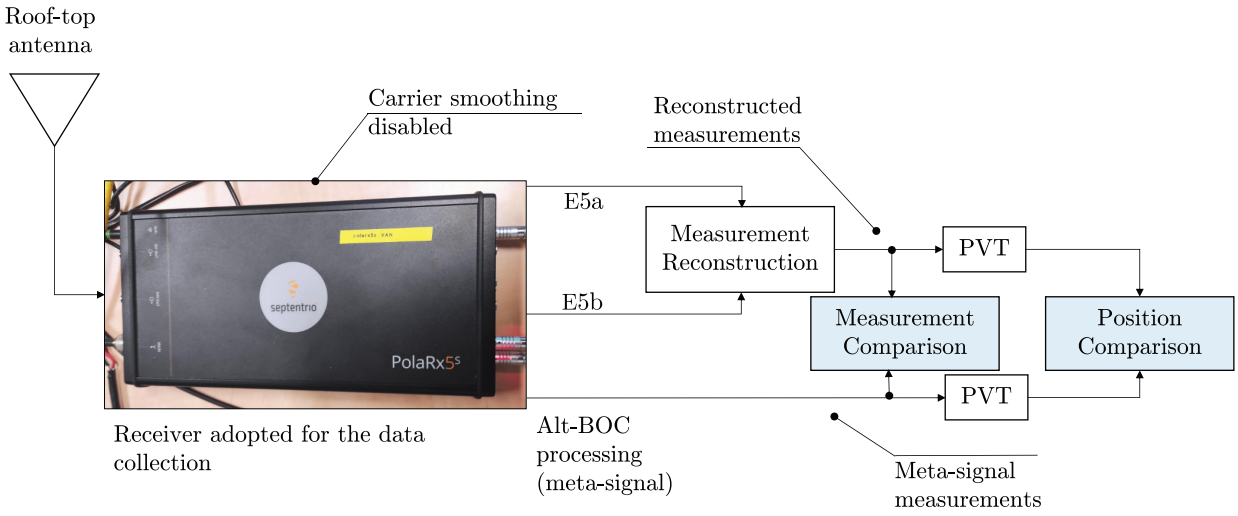

FIGURE 4 Schematic representation of the experimental setup and processing scheme adopted for the data collection and analysis

full Alt-BOC modulation. It processes the Alt-BOC modulation using a previously discussed approach (Simsky et al., 2005; Sleewaegen et al., 2004). This approach utilizes the E5a and E5b pilot components to generate a single wideband signal replica. In this manner, it was possible to record both sideband and meta-signal measurements. For the test, carrier smoothing was disabled to avoid filtering pseudoranges with carrier-phase observations.

Pseudoranges and carrier phases from the sideband components, the E5a and E5b signals, were used to reconstruct meta-signal measurements using the relationships derived in the previous sections. These measurements were then compared with the observations obtained for the full Alt-BOC signal.

Analysis was also conducted in the position domain and different solutions were compared. In particular, a custom software was developed to compute the final user position considering different processing options:

1. A position, velocity, and time (PVT) solution using Alt-BOC pseudoranges: This option corresponds to the case in which meta-signal processing is adopted and the Alt-BOC is processed as a single wideband signal.
2. A PVT solution using individual sideband components: In this case, two separate solutions are obtained for the E5a and E5b components. In both cases, only measurements from the pilot components were considered.
3. A PVT solution obtained using raw pseudoranges reconstructed from the sideband components: In this case, the pseudoranges from the E5a and E5b signals are linearly combined and used to compute the final PVT solution.
4. A PVT solution obtained using final pseudoranges computed using carrier and code measurements from the two sideband components: In this case, the meta-signal final pseudoranges are constructed from both code and carrier observations obtained from the two sideband components.

In all cases, a weighted least squares (WLS) solution was adopted in which the weights were computed as a function of the satellite elevation.

5 | EXPERIMENTAL RESULTS

In this section, results obtained from processing the measurements collected according to the methodology described in Section 4 are presented. Findings in the measurement domain are detailed first, followed by an analysis in the position domain.

5.1 | Measurement Domain Analysis

Carrier-phase observations obtained from Alt-BOC processing have been compared with measurements reconstructed from the E5a and E5b signals using Equation (13) and, in particular, differences have been computed:

$$\Delta\varphi = \varphi^{Alt-BOC} - \varphi^{rec} = \varphi^{Alt-BOC} - \frac{1}{2}\left(\varphi^{E5b} + \varphi^{E5a}\right) \tag{26}$$

where $\varphi^{Alt-BOC}$ are the carrier-phase measurements from the full Alt-BOC modulation expressed in cycles, φ^{E5b} and φ^{E5a} are carrier-phase observations from the sideband components, and $\varphi^{rec} = \frac{1}{2}\left(\varphi^{E5b} + \varphi^{E5a}\right)$ is the meta-signal carrier phase reconstructed using Equation (13).

Since $\varphi^{Alt-BOC}$ and φ^{rec} can differ for an integer multiple of half-cycles, the following corrected phase differences have been considered:

$$\overline{\Delta\varphi} = \Delta\varphi - \frac{1}{2}\,\mathrm{round}\left(2\Delta\varphi\right) \tag{27}$$

where half-cycles have been removed. Corrected differences from Equation (27) are shown in Figure 5: They all overlap on the same mean value and are characterized by reduced standard deviations. This indicates the equivalence of the two types of measurements: those from the Alt-BOC and those reconstructed from the sideband components. A perfect reconstruction (i.e., zero corrected differences) cannot be expected because the measurements from the three channels, the Alt-BOC and the two sidebands, are generated from different tracking loops with different processing architectures. GNSS signals are noisy and noise components are propagated differently through the receiver depending on the processing mode selected. The fact that the corrected differences are not zero-meaned simply indicates that a different processing delay is introduced between the Alt-BOC and the reconstructed measurements. In a final position solution, this mean, which is constant between the corrected differences, will be absorbed by the clock bias term without impacting the position coordinates. The mean of corrected differences from all available satellites is $7.6\cdot10^{-3}$ cycles (approximately 1.9 mm), whereas the average standard deviation is $1.36\cdot10^{-3}$ cycles (approximately 0.34 mm). Differences in standard deviations are primarily due to satellite elevations, with the larger values observed for low elevation satellites. However,

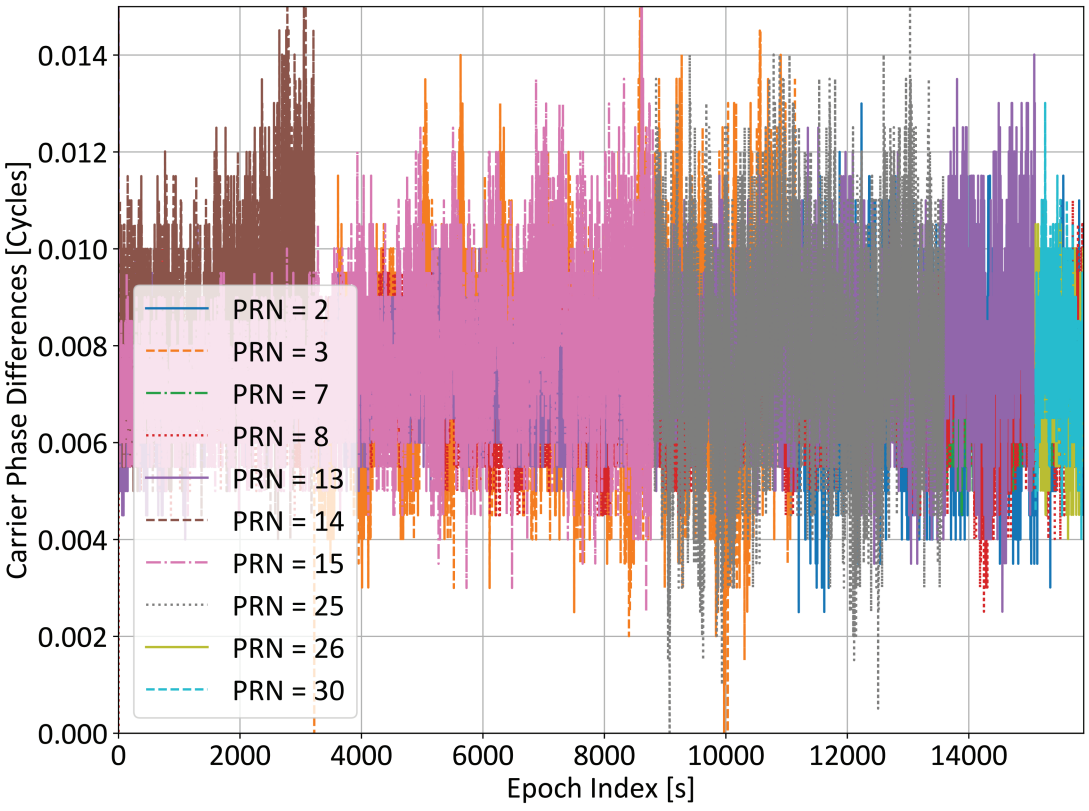

FIGURE 5 Corrected differences obtained by comparing Alt-BOC carrier phases with observations reconstructed from the E5a and E5b components; the data is from the PolarRx5s receiver.

these values are very small and support the validity of the reconstruction formula for carrier-phase measurements.

The statistical properties of the corrected differences are further analyzed in Figure 6, which provides the box plot of the corrected difference considered in Figure 5. The horizontal lines inside the boxes represent the median values of the corrected differences: All the medians are aligned and differ in the few tens of millicycles. The horizontal sides of the boxes are the 25th and 75th percentiles of the corrected differences and the boxes represent their interquartile range. The reduced size of these boxes confirms a low dispersion of the corrected differences. External horizontal segments are the maximum and minimum values, whereas diamond markers represent outliers. The outliers occur when the receiver gains or is about to lose its lock on a specific signal: Without stable tracking, the measurements are affected by large errors and the corrected differences assume large values that should be discarded from the analysis. This fact clearly emerges in Figure 5. Consider, for example, the observations from the satellite with pseudorandom number (PRN) 14: the satellite is at a low elevation and loses signal lock after about 3,000 s from the start of the experiment. These conditions make this satellite have a larger interquartile range but fewer outliers.

A similar analysis has been conducted for the pseudoranges and their differences:

$$\Delta\rho = \rho^{Alt-BOC} - \rho^{+} \tag{28}$$

In Equation (28), $\rho^{Alt-BOC}$ are the pseudoranges obtained from full Alt-BOC processing and ρ^{+} are the measurements reconstructed using Equation (24) as well as the pseudoranges from the E5a and E5b signals. These differences are depicted in Figure 7. As for the carrier-phase case, all of the pseudoranges have the same mean

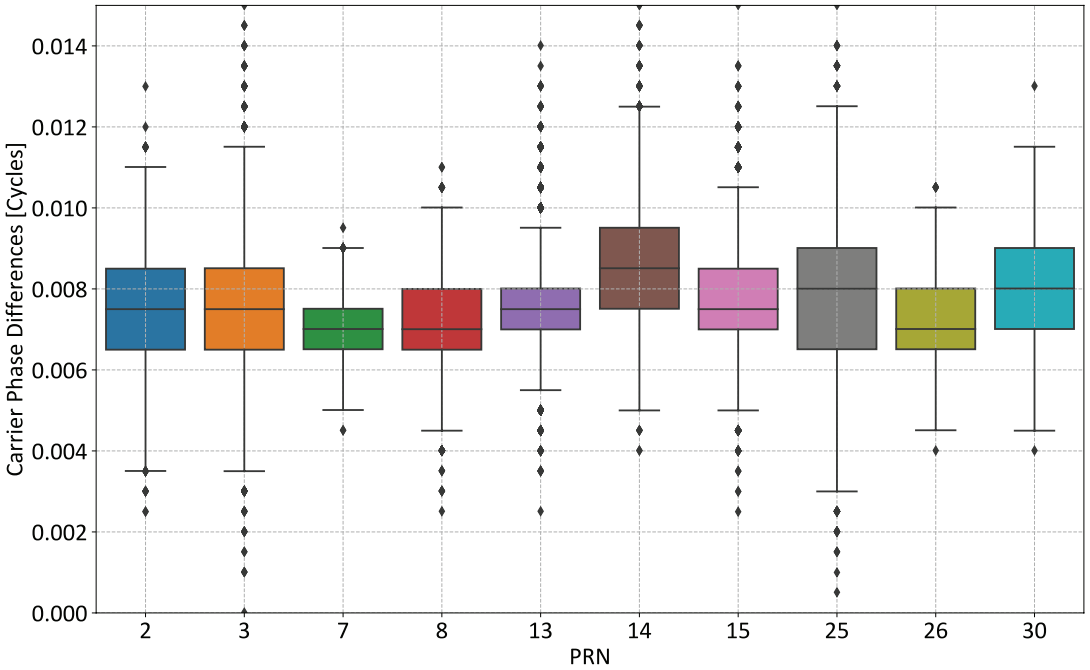

FIGURE 6 Box plots of the corrected differences considered in Figure 5: Central lines inside the boxes represent the median values, whereas the horizontal sides of the boxes are the 25 and 75 percentiles. External horizontal segments are the maximum and minimum values, whereas diamond markers represent outliers.

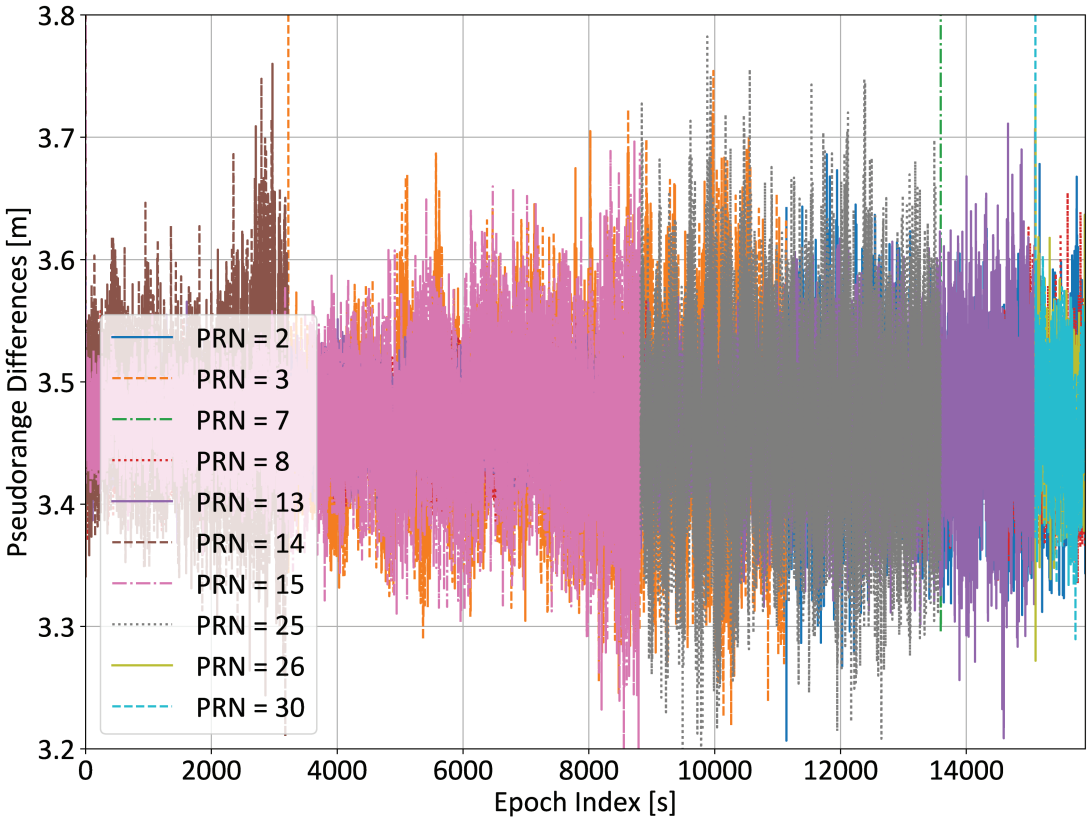

FIGURE 7 Differences between Alt-BOC pseudoranges and final observations reconstructed from E5a and E5b pseudoranges and carrier phases; data was collected from the PolarRx5s receiver.

and a reduced standard deviation. The common mean term, about 3.47 meters, will be absorbed by the clock bias without impacting the position solution. The standard deviations range from 3 to 8 cm and depend on the satellite elevation and signal strength.

The statistical properties of the pseudorange differences are further analyzed in Figure 8: All of the medians assume close values. Moreover, the interquartile boxes have a reduced extent: Alt-BOC and reconstructed pseudoranges differ only for small random variations and for a constant bias, which is derived from the different processing chains.

These results confirm the validity of the reconstruction formulas derived for the meta-signal carrier phases and pseudoranges.

5.2 | Position Domain Analysis

As discussed in Section 4, Alt-BOC, sideband, and reconstructed pseudoranges have been used to compute different position solutions, which have been converted into an east-north-up (ENU) frame centered with respect to the actual antenna location. Thus, deviations from zero indicate actual position errors in the different components. The scatter plots of the east and north position errors are provided in Figure 9 for the various configurations. Single band position solutions are the noisiest, reflected by the larger spread of the

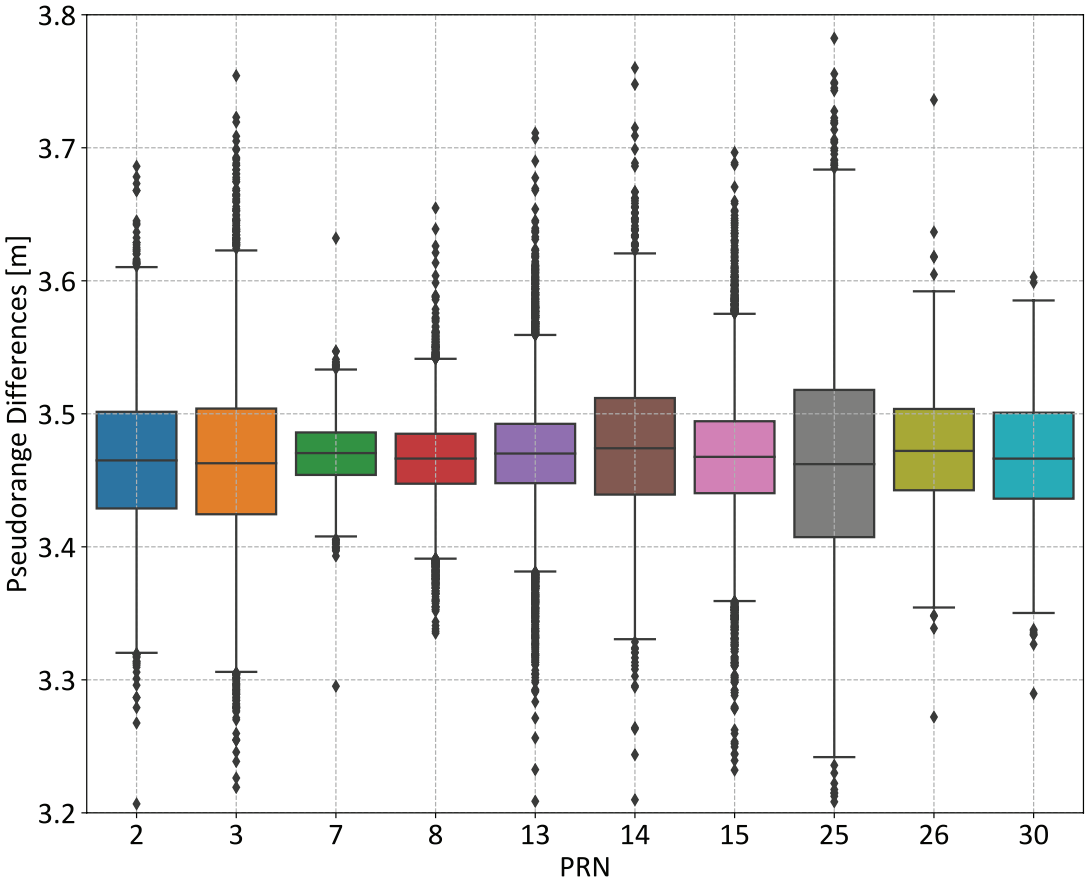

FIGURE 8 Box plots of the pseudorange differences considered in Figure 7: Central lines inside the boxes represent the median values, whereas the horizontal sides of the boxes are the 25th and 75th percentiles. External horizontal segments are the maximum and minimum values, whereas diamond markers represent outliers.

corresponding scatterplots. The use of average (raw) pseudoranges, computed according to Equation (23), provides some improvement as compared to individual sideband processing. The scatterplot of the solution obtained using raw pseudoranges is labeled in Figure 9 as *E5 Mean*. As expected, the best performance is achieved when full Alt-BOC processing is adopted: The corresponding scatter plot has the lowest spread in Figure 9. The solutions obtained using final pseudoranges computed according to Equation (24) practically coincide with those obtained using Alt-BOC pseudoranges. This result further confirms the findings discussed in the previous section: The Alt-BOC and final pseudoranges lead to practically coinciding position solutions and the constant bias observed in Section 5.1 is absorbed by the clock bias component.

The vertical components of the position solutions are analyzed in Figure 10. All of the configurations are analyzed in the upper box of the figure whereas the solutions for the Alt-BOC and for the final pseudoranges are compared in the lower box. While the vertical components show slightly increased variations, the figure further supports the findings obtained for the horizontal channel. The Alt-BOC solutions and the solutions obtained using final pseudoranges computed from the sideband components practically coincide, confirming the validity of the reconstruction formulas derived in the paper.

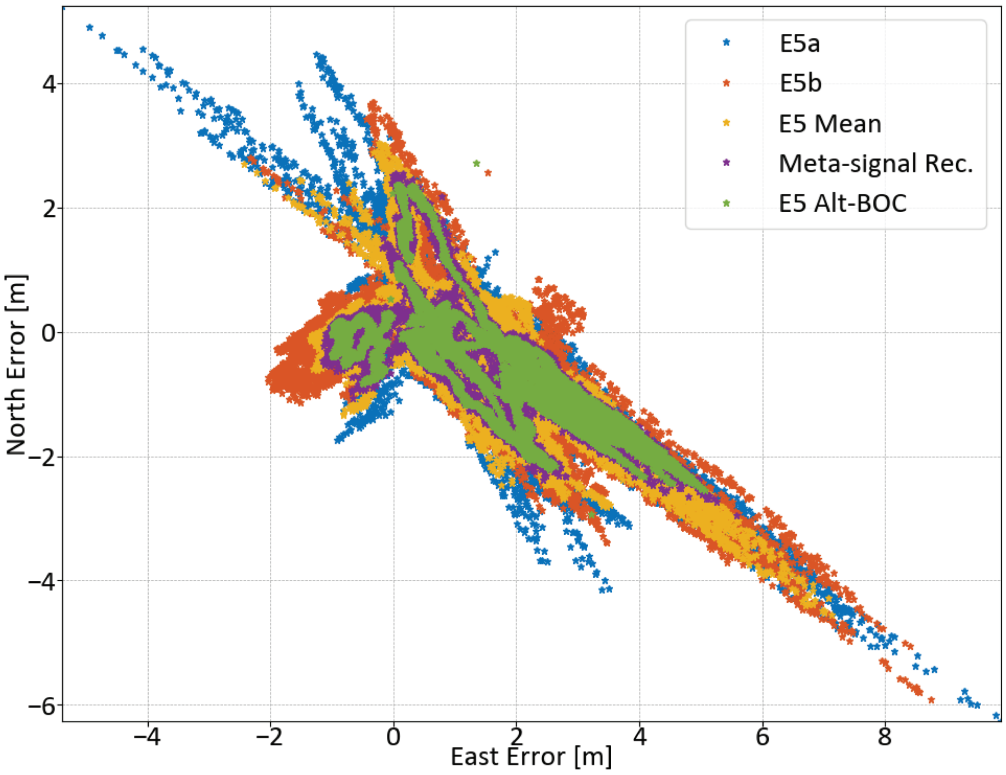

FIGURE 9 Scatterplot of the east/north position errors for the different configurations considered

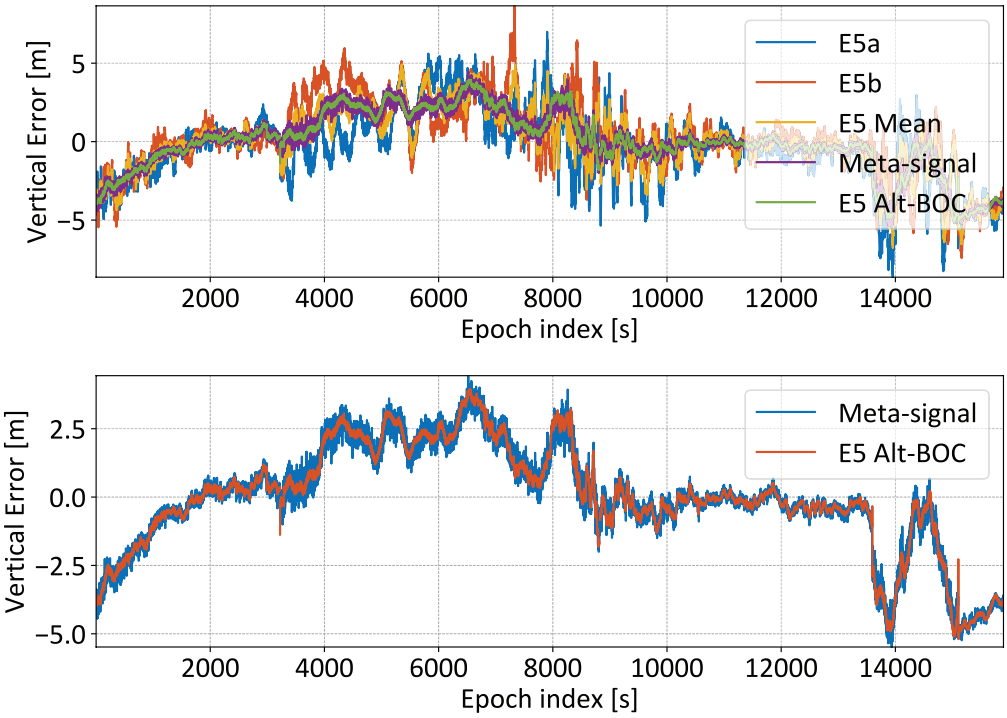

FIGURE 10 Up position errors for the different configurations as a function of time: The upper box represents all solutions while the bottom box is a comparison between the Alt-BOC solutions and the ones obtained using final pseudoranges computed from the sideband components.

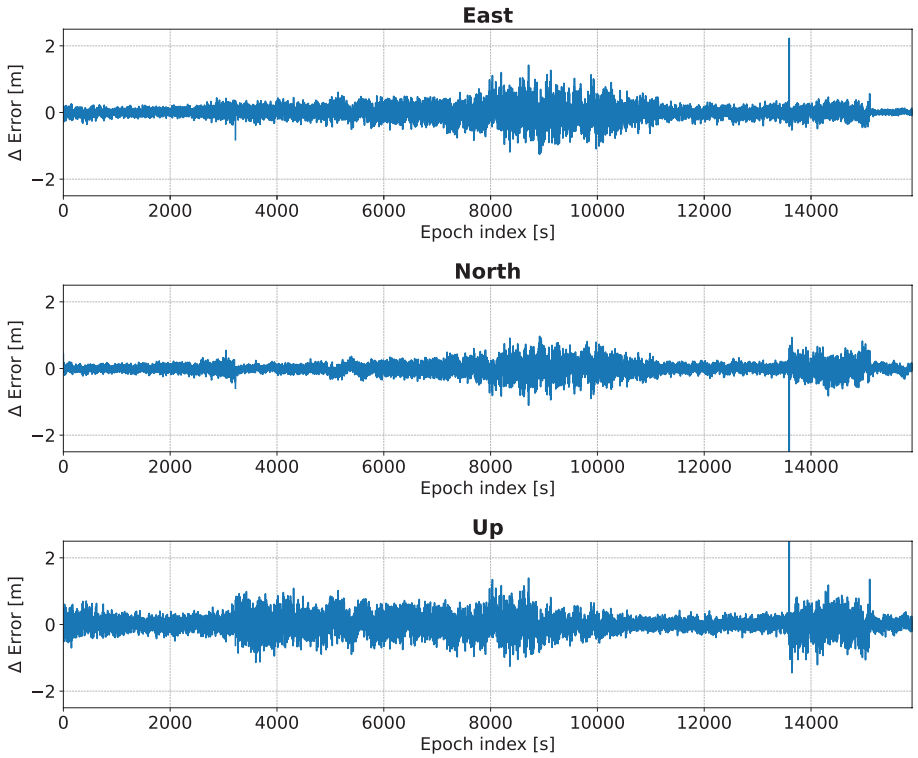

FIGURE 11 Differences between position solutions computed using pseudoranges obtained from full Alt-BOC processing and final pseudoranges reconstructed from the sideband components.

The solutions obtained using Alt-BOC and reconstructed final pseudoranges are further analyzed in Figure 11, which shows the differences between the east, north, and up components determined for these two configurations. The figure further confirms that the two solutions have the same mean and result in zero-mean differences. The magnitude of the differences changes as a function of the geometric conditions of the satellites in view. For example, in the last 700 epochs of the test, five satellites were tracked. In this part of the test, differences are further reduced.

The histograms of the differences of the position solutions computed using pseudoranges obtained from full Alt-BOC processing and final pseudoranges reconstructed from the sideband components are provided in Figure 12. The mean and standard deviations of the differences are also provided. Mean differences are below one cm for all three components. The worst standard deviation is observed for the vertical component. This standard deviation, however, does not exceed 25 cm.

As previously discussed for the observations, perfect reconstruction of the Alt-BOC measurements should not be expected: The two sets of measurements are obtained using different signal processing blocks with different tracking loops and processing parameters. The results provided in this section show that Equation (24) is effective in reconstructing pseudoranges that, on average, lead to the same position solution obtained using Alt-BOC processing. Residual differences are random in nature and are characterized by a reduced standard deviation, which is always lower than 25 cm.

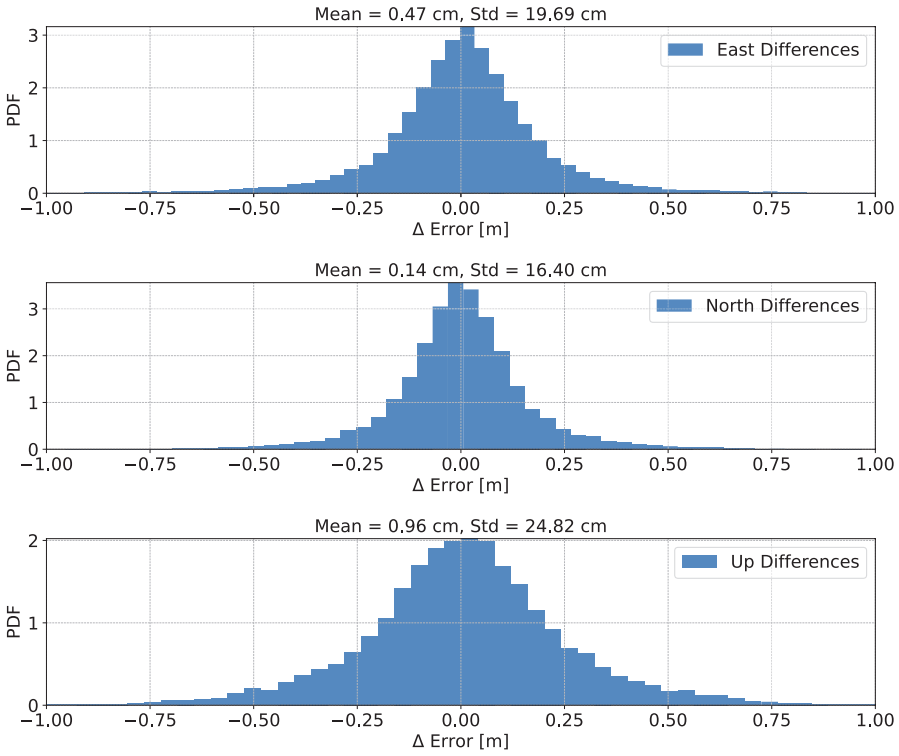

FIGURE 12 Histograms of the differences of the position solutions computed using pseudoranges obtained from full Alt-BOC processing and final pseudoranges reconstructed from the sideband components: The top box represents the east component, the middle box represents the north component, and the bottom box represents the up component.

6 | CONCLUSION

In this work, the observations obtained from the processing of GNSS meta-signals have been characterized in terms of pseudoranges and carrier phases of the meta-signal sideband components. A DPE-like architecture has been considered in which code, carrier, and subcarrier measurements are generated when processing a GNSS meta-signal. This architecture is required to solve the code ambiguity problem and obtain unambiguous pseudoranges.

The theoretical framework developed shows that the meta-signal carrier phase is the narrow-lane combination of the carrier-phase observations from the two sideband components. Similarly, the meta-signal subcarrier phase is the wide-lane combination of the sideband carrier phases. Finally, meta-signal pseudoranges are a combination of both sideband pseudoranges and carrier phases. In this respect, a meta-signal pseudorange cannot be considered a pure code measurement because its final accuracy is determined by the wide-lane combination of the sideband carrier-phase measurements. Experiments conducted using measurements from full Alt-BOC processing and from its sidebands, the Galileo E5a and E5b signals, have been used to support theoretical findings. A good agreement between empirical results has been obtained showing that Alt-BOC carrier phases can be recovered from the carrier phases of its sideband components. Similar results were obtained for the pseudoranges that can be reconstructed from E5a and E5b observations.

Analysis was also conducted in the position domain: The position solutions obtained from the reconstructed measurements have the same mean as those computed from Alt-BOC observations. Residual differences are zero-mean with a

standard deviation lower than 25 cm. These results support the theoretical findings derived in the paper.

The relationships derived in the paper shed light on the nature of the measurements generated through GNSS meta-signal processing and provide important considerations for the design and processing of future GNSS signals that will be obtained by adding new components to existing modulations.

AUTHOR CONTRIBUTIONS

Dr. Borio contributed to the theoretical developments and to the analysis of the GNSS measurements. Dr. Gioia performed the data collection and conducted the experimental analysis. Both authors drafted and reviewed the manuscript.

CONFLICT OF INTEREST

The authors declare no potential conflicts of interest.

REFERENCES

Betz, J. W. (2001). Binary offset carrier modulations for radionavigation. *NAVIGATION*, *48*(4), 227–246. https://doi.org/10.1002/j.2161-4296.2001.tb00247.x

Betz, J. W., & Kolodziejski, K. R. (2009). Generalized theory of code tracking with an early-late discriminator part I: lower bound and coherent processing. *IEEE Transactions on Aerospace and Electronic Systems*, *45*(4), 1538–1556. https://doi.org/10.1109/TAES.2009.5310316

Borio, D. (2014, August). Double phase estimator: new unambiguous binary offset carrier tracking algorithm. *IET Radar, Sonar & Navigation*, *8*(7), 729–741. https://doi.org/10.1049/iet-rsn.2013.0306

Borio, D. (2017, October). Coherent side-band BOC processing. *IET Radar, Sonar & Navigation*, *11*(10), 1455–1466. https://doi.org/10.1049/iet-rsn.2016.0245

Borio, D., & Gioia, C. (2022, January). GNSS meta-signals, dual-frequency combinations and the double phase estimator. *Proc. of the 2022 International Technical Meeting of the Institute of Navigation,* Long Beach, CA, 1015–1026. https://doi.org/10.33012/2022.18191

Das, P., Ortega, L., Vilá-Valls, J., Vincent, F., Chaumette, E., & Davain, L. (2020). Performance limits of GNSS code-based precise positioning: GPS, Galileo & meta-signals. *Sensors*, *20*(8), 2196. https://doi.org/10.3390/s20082196

Deng, C., Tang, W., Cui, J., Shen, M., Li, Z., Zou, X., & Zhang, Y. (2018). Triple-frequency code-phase combination determination: a comparison with the Hatch-Melbourne-Wübbena combination using BDS signals. *Remote Sensing*, *10*(2), 353. https://doi.org/10.3390/rs10020353

Feng, T., Kai, Z., & Liang, C. (2016). Unambiguous tracking of BOC signals using coherent combination of dual sidebands. *IEEE Communications Letters*, *20*(8), 1555–1558. https://doi.org/10.1109/LCOMM.2016.2569520

Fine, P., & Wilson, W. (1999, January). Tracking algorithm for GPS offset carrier signals. *Proc. of the 1999 National Technical Meeting of the Institute of Navigation*, San Diego, CA, 671–676. https://www.ion.org/publications/abstract.cfm?articleID=719

Gao, Y., Yao, Z., & Lu, M. (2020a). A coherent processing technique with high precision for BDS B1I and B1C signals. In J. Sun, C. Yang, & J. Xie (Eds.), *China Satellite Navigation Conference (CSNC) 2020 Proceedings: Vol. 1* (pp. 537–550). Springer. https://doi.org/10.1007/978-981-15-3707-3_51

Gao, Y., Yao, Z., & Lu, M. (2020b). High-precision unambiguous tracking technique for BDS B1 wideband composite signal. *NAVIGATION, 67*(3), 633–650. https://doi.org/10.1002/navi.377

García-Molina, J. A. (2021). Unambiguous meta-signal processing: a path to code-based high-accuracy PNT. *Inside GNSS*, 50–55. https://insidegnss.com/unambiguous-meta-signal-processing-a-path-to-code-based-high-accuracy-pnt/

García-Molina, J. A., & Fernández-Rubio, J. A. (2019). Collective unambiguous positioning with high-order BOC signals. *IEEE Transactions on Aerospace and Electronic Systems*, *55*(3), 1461–1473. https://doi.org/10.1109/TAES.2018.2871512

Hameed, M. S., Woerz, T., Pany, T., Wendel, J., Paonni, M., & Senni, T. (2021). Demonstration of meta-signal positioning using LAMBDA ambiguity fixing method within a bit-true simulation. *Proc. of the 34th International Technical Meeting of the Satellite Division of the Institute of Navigation (ION GNSS+ 2021),* St. Louis, MO, 2819–2837. https://doi.org/10.33012/2021.18011

Hodgart, M. S., & Blunt, P. D. (2007, August). Dual estimate receiver of binary offset carrier modulated signals for global navigation satellite systems. *Electronics Letters*, *43*(16), 877–878. https://doi.org/10.1049/el:20071101

Hodgart, M. S., Blunt, P. D., & Unwin, M. (2008). Double estimator: A new receiver principle for tracking BOC signals. *Inside GNSS*, 26–36. https://insidegnss.com/double-estimator-a-new-receiver-principle-for-tracking-boc-signals/

Hofmann-Wellenhof, B., Lichtenegger, H., & Collins, J. (2001). *Global Positioning System: theory and practice* (5th ed.). Springer. https://doi.org/10.1007/978-3-7091-6199-9

Issler, J. -L., Paonni, M., & Eissfeller, B. (2010). Toward centimetric positioning thanks to L- and S-band GNSS and to meta-GNSS signals. *2010 5th ESA Workshop on Satellite Navigation Technologies and European Workshop on GNSS Signals and Signal Processing (NAVITEC),* Noordwijk, Netherlands. https://doi.org/10.1109/NAVITEC.2010.5708075

Kaplan, E. D., & Hegarty, C. (Eds.). (2017). *Understanding GPS/GNSS: principles and applications* (3rd ed.). Artech House Publishers. https://ieeexplore.ieee.org/document/9100468

Lestarquit, L., Artaud, G., & Issler, J. -L. (2008, September). AltBOC for dummies or everything you always wanted to know about AltBOC. *Proc. of the 21st International Technical Meeting of the Satellite Division of the Institute of Navigation (ION GNSS 2008)*, Savannah, GA, 961–970. https://www.ion.org/publications/abstract.cfm?articleID=8018

Li, B. (2018, February). Review of triple-frequency GNSS: ambiguity resolution, benefits and challenges. *Journal of Global Positioning Systems*, *16*, 1. https://doi.org/10.1186/s41445-018-0010-y

Nardin, A., Dovis, F., & Motella, B. (2020, November). Impact of non-idealities on GNSS meta-signals processing. *2020 European Navigation Conference (ENC),* Dresden, Germany. https://doi.org/10.23919/ENC48637.2020.9317365

Ortega, L., Medina, D., Vilà-Valls, J., Vincent, F., & Chaumette, E. (2020). Positioning performance limits of GNSS meta-signals and HO-BOC signals. *Sensors*, *20*(12), 3586. https://doi.org/10.3390/s20123586

Pany, T., & Yang, C. (2017, January). Code and carrier tracking for spectrally asymmetric signals. *Proc. of the 2017 International Technical Meeting of the Institute of Navigation*, Monterey, CA, 335–346. https://doi.org/10.33012/2017.14950

Paonni, M., Curran, J. T., Bavaro, M., & Fortuny-Guasch, J. (2014, September). GNSS meta signals: coherently composite processing of multiple GNSS signals. *Proc. of the 27th International Technical Meeting of the Satellite Division of the Institute of Navigation (ION GNSS+)*, Tampa, FL, 2592–2601. https://www.ion.org/publications/abstract.cfm?articleID=12322

Richert, T., & El-Sheimy, N. (2007). Optimal linear combinations of triple frequency carrier phase data from future global navigation satellite systems. *GPS Solutions*, *11*, 11–19. https://doi.org/10.1007/s10291-006-0024-x

Schwalm, C., Enneking, C., & Thoelert, S. (2020, November). Ziv-zakai bound and multicorrelator compression for a Galileo E1 meta-signal. *2020 European Navigation Conference,* Dresden, Germany. https://doi.org/10.23919/ENC48637.2020.9317389

Simsky, A., Sleewaegen, J. -M., De Wilde, W., & Wilms, F. (2005, July). Galileo receiver development at Septentrio. *2005 European Navigation Conference (ENC)*, Minich, Germany. https://www.academia.edu/1975615/Galileo_receiver_development_at_Septentrio

Sleewaegen, J. -M., De Wilde, W., & Hollreiser, M. (2004). Galileo AltBOC receiver. Septentrio. https://www.septentrio.com/sites/default/files/2019-12/Septentrio-Paper-2014-Sleewaegen-De-Wilde-Galileo-AltBOC-GNSS-Receiver.pdf

Tsui, J. B. -Y. (2004). *Fundamentals of global positioning system receivers: a software approach* (2nd ed.). Wiley. https://www.wiley.com/en-us/Fundamentals+of+Global+Positioning+System+Receivers%3A+A+Software+Approach%2C+2nd+Edition-p-9780471712572

Van Dierendonck, A. (1997). Global positioning system theory and applications. In B. W. Parkinson & J. J. Spilker Jr. (Eds.), *Global positioning system: theory and applications* (Vol. 1, pp. 329–407). American Institute of Aeronautics & Astronautics. https://doi.org/10.2514/4.866388

Wang, C., Cui, X., Ma, T., Zhao, S., & Lu, M. (2017). Asymmetric dual-band tracking technique for optimal joint processing of BDS B1I and B1C signals. *Sensors*, *17*(10), 2360. https://doi.org/10.3390/s17102360

Yang, C. (2016). Sharpen the correlation peak: A novel GNSS receiver architecture with variable IF correlation. *NAVIGATION, 63*(3), 249–265. https://doi.org/10.1002/navi.147

Yao, Z., Gao, Y., Gao, Y., & Lu, M. (2017). Generalized theory of BOC signal unambiguous tracking with two-dimensional loops. *IEEE Transactions on Aerospace and Electronic Systems*, *53*(6), 3056–3069. https://doi.org/10.1109/TAES.2017.2726878

Zhang, W., Yao, Z., & Lu, M. (2019, July). WHAT: wideband high-accuracy joint tracking technique for BDS B1 composite signal. *2019 IEEE 9th International Conference on Electronics Information and Emergency Communication (ICEIEC)*, Beijing, China. https://doi.org/10.1109/ICEIEC.2019.8784630

How to cite this article: Borio, D., & Gioia, C., (2023). Reconstructing GNSS meta-signal observations using sideband measurements. *NAVIGATION, 70*(1). https://doi.org/10.33012/navi.558